Heliyon 9 (2023) e17711

Contents lists available at ScienceDirect

Heliyon

journal homepage: www.cell.com/heliyon

Tetraspanin CD63 reduces the progression and metastasis of head and neck squamous cell carcinoma via KRT1-mediated cell cycle arrest

Qiang Huang [a,b,1], Yu-Jie Shen [a,b,1], Chi-Yao Hsueh [a,b,1], Yi-Fan Zhang [a,b,1], Yang Guo [a,b], Xiao-Hui Yuan [a,b], Chun-Yan Hu [c], Jiao-Yu Li [d], Lei Tao [a,b], Hong-Li Gong [a,b,*], Ming Zhang [a,b,**], Liang Zhou [a,b,***]

[a] Department of Otorhinolaryngology, Eye & ENT Hospital, Fudan University, Shanghai 200031, China
[b] Shanghai Key Clinical Disciplines of Otorhinolaryngology, Shanghai 200031, China
[c] Department of Pathology, Eye & ENT Hospital, Fudan University, Shanghai 200031, China
[d] Department of Pediatric, Xinhua Hospital, Shanghai Jiaotong University School of Medicine, Shanghai 200092, China

ARTICLE INFO

Keywords:
CD63
KRT1
Metastasis
HNSCC
Cell cycle arrest

ABSTRACT

Despite the fact that metastasis is the leading cause of death in patients with head and neck squamous cell carcinoma, fundamental questions about the mechanisms that enable or inhibit metastasis remain unanswered. Tetraspanin CD63 has been linked to tumor progression and metastasis. However, few studies have examined the role of CD63 in HNSCC. In this study, we discovered that CD63 levels were abnormally altered in HNSCC tissue compared to adjacent tissue (n = 69 pairs), and that this was linked to prognosis. Through functional *in vitro* and *in vivo* experiments, the roles of CD63 in HNSCC were confirmed. Overexpression of CD63 inhibited the progression and metastasis of HNSCC cells. Using mass spectrometry and co-immunoprecipitation assays, we discovered that KRT1 could be a direct interacting partner of CD63. Furthermore, both CD63 and KRT1 expression was significantly decreased in metastatic tissue compared with primary tumor tissue (n = 13 pairs), suggesting that CD63 and KRT1 play a role in reducing the metastasis of HNSCC. In summary, we reveal a previously unrecognized role of CD63 in regulating KRT1-mediated cell cycle arrest in HNSCC cells, and our findings contribute to defining an important mechanism of HNSCC progression and metastasis.

1. Introduction

Head and neck squamous cell carcinoma (HNSCC) accounts for the vast majority of head and neck cancers [1]. The incidence of HNSCC has increased by approximately 30% since 1990, and it is now the seventh most common cancer worldwide [2]. Meanwhile,

* Corresponding author. Department of Otorhinolaryngology, Eye & ENT Hospital, Fudan University, Shanghai 200031, China.
** Corresponding author. Department of Otorhinolaryngology, Eye & ENT Hospital, Fudan University, Shanghai 200031, China.
*** Corresponding author. Department of Otorhinolaryngology, Eye & ENT Hospital, Fudan University, Shanghai 200031, China.
E-mail addresses: gonghlent@126.com, hongli.gong@fdeent.org (H.-L. Gong), zmzlm@163.com, ming.zhang@fdeent.org (M. Zhang), zhoulent@126.com, liang.zhou@fdeent.org (L. Zhou).
[1] These authors contributed equally to this work.

https://doi.org/10.1016/j.heliyon.2023.e17711
Received 18 July 2022; Received in revised form 20 June 2023; Accepted 26 June 2023
Available online 4 July 2023

HNSCC patients are at a high risk of cervical lymph node metastases [3]. Cervical lymph node involvement is a well-known prognostic marker for HNSCC, and the presence of positive lymph nodes is thought to be a predictor of poor patient outcomes [4]. However, fundamental questions regarding the mechanisms that facilitate or restrain dissemination to local or distant metastases remain unrevealed.

Epigenetic alterations like methylation of tumor suppressor genes or oncogenes have been associated with HNSCC. Epigenetic drugs like DNA methyltransferase-1 (DNMT1) inhibitors have been exhibited positive effects in cancer treatment. Yang et al. found the expression level of DNMT1 was correlated with the immunosuppressive molecules and tumor-promoter such as VISTA, PD-L1, B7–H4, and PAK2, indicating a poor prognosis in oral squamous cell carcinoma (OSCC) [5]. For sure, in addition to that, inflammation contributes to HNSCC initiation, progression, and immune escape. Tang et al. systemically analyzed the distribution profiles and phenotypic features of neutrophils and other inflammatory immune cell population, and found that tumor-infiltrating PD-L1+ neutrophils induced by laryngeal squamous cell carcinoma (LSCC)-derived GM-CSF weaken T cell proliferation and activation in the inflammatory microenvironment of LSCC and predict poor prognosis [6].

Tetraspanins are transmembrane proteins, composed of outer loops and short N- and C-terminal tails with four transmembrane domains [7]. They form complexes known as tetraspanin-enriched microdomains by interacting with other tetraspanins and a variety of transmembrane and cytosolic proteins that are required for their function [8,9]. The tetraspanin protein CD63 has recently been described as a key factor in extracellular vesicles (EVs) production and endosomal cargo sorting [10,11]. Mounting evidence suggests that CD63 is also involved in tumor progression. The first work to link CD63 to cancer research can be traced back to melanoma research [12–15]. However, there is no consensus yet about whether CD63 promotes or blocks tumorigenesis. Lupia et al. established that CD63 is highly expressed in early melanoma and decreased in advanced lesions. CD63-silenced melanoma cells showed increased motor capacity and aggressivity by regulating epithelial–mesenchymal transition (EMT)-related genes, suggesting that it is a possible suppressor of melanoma progression [9]. Kudo et al. showed the potential of cell surface CD63 to sensitize melanoma cells to BRAF inhibitor PLX4032 and to reduce the proliferation of PLX4032-resistant cells [16]. Yu et al. found that in hepatocellular carcinoma, overexpression of CD63 inhibited tumor cell proliferation and migration, whereas knockdown of CD63 promoted these phenotypes, possibly through CD63 regulation of IL-6/IL-27-STAT3 axis [17]. On the contrary, other studies have shown the opposite. Seubert et al. found that CD63 induced a more epithelial-like phenotype accompanied by increased E-cadherin expression and acted as a pro-metastatic factor [18]. Furthermore, Schoeps et al. found that tumor-derived protein tissue inhibitor of metalloproteinases-1 (TIMP1) directly triggered formation of neutrophil extracellular traps, which was dependent on the interaction of TIMP1 with its receptor CD63 and subsequent ERK signaling [19]. However, few studies have shown the role of CD63 in HNSCC.

This study aimed to clarify the role of CD63 in the progression and metastasis of HNSCC *in vitro* and *in vivo*, to detect the correlation with clinical characteristics of patients with HNSCC, and to study the proteins that interact with CD63, exploring the mechanism of CD63-related phenotype changes in HNSCC.

2. Methods and materials

2.1. Patient tissue and ethics approval

Tissue microarray was obtained from 80 patients (among the 160 cores, 22 were lost during processing) diagnosed with HNSCC pathologically after surgery from July 2014 to March 2018 (FDEENT TMA); paired fresh pathological specimens were obtained from 124 patients (including 13 pairs of primary and metastatic tissue) from March 2019 to June 2021 from the Department of Otorhinolaryngology, Eye & ENT Hospital of Fudan University. The inclusion criterion was as follows: confirmation of HNSCC by experienced pathologists and classification of tumor stage according to the AJCC cancer staging manual (8th) with complete clinical, imaging, laboratory, and pathological data. The exclusion criteria were as follows: (a) histopathological confirmation of multiple types of primary HNSCC, (b) preoperative treatment with approaches such as radiotherapy or chemotherapy, or (c) infectious disease or autoimmune disease [20]. All participants provided written informed consent forms. This study was approved by the Clinical Research Ethics Committee of the Eye & ENT Hospital of Fudan University (NO. KJ2008–01). Commercial TMA (including 83 HNSCC tissue) was purchased from Superbiotek (ZL-HNT1021, Shanghai, China), which detailed information can be obtained from Supplementary Table 1.

2.2. Cell culture

HuLa-PC, a cell line derived from posterior commissure of the larynx, was obtained from ATCC (Gaithersburg, Maryland) and cultured in Dermal Cell Basal Medium (ATCC® PCS-200-030™) supplied with Keratinocyte Growth Kit (ATCC® PCS-200-040™). The HNSCC cell line AMC-HN8 was a kind gift from Professor Sang Yoon Kim of Samsung Medical Center, Korea. Tu686 was obtained from Central South University (Hunan, China). FaDu and Detroit562 were obtained from the Cell Bank of the Shanghai Institute of Cells, Chinese Academy of Science (Shanghai, China). AMC-HN8 was cultured in RPMI-1640 (HyClone, Logan, UT). Tu686, FaDu, and Detroit562 were cultured in DMEM (Gibco, Grand Island, NY). The growth medium contained 1% penicillin-streptomycin (Genom Biotechnology, China) and 10% fetal bovine serum (FBS; Gibco, Grand Island, NY). The cells were incubated with 5% CO_2 at 37 °C. All HNSCC cell lines were tested for potential mycoplasma contamination.

2.3. RNA isolation and qRT-PCR

Total RNA was isolated from tissue and cells with TRIzol reagent (Invitrogen, Thermo Fisher Scientific), measured by a microspectrophotometer Nanodrop 2000 (Thermo Fisher Scientific), with the ratio of OD260/OD280 > 1.8 and then reversed-transcribed using an Evo M-MLV Mix Kit with gDNA Clean for qPCR (AG11728, Accurate Biology, Hunan, China). qRT-PCR was conducted using SYBR® Green Premix Pro Taq HS qPCR Kit (AG11718, Accurate Biology, Hunan, China) with the ABI 7500 Real-Time PCR System (Life Technologies, Shanghai, China) using the $2^{-\Delta\Delta Ct}$ method. The primers were synthesized by Sangon Biotech (Shanghai). The housekeeping genes GAPDH was used as internal references to normalize gene expression. The sequences of primers used are as follows: CD63: ATGCAGGCAGATTTTAAGTGCT (forward), GTTCTTCGACATGGAAGGGATTT (reverse); KRT1: AGAGTGGACCAACTGAAGAGT (forward), ATTCTCTGCATTTGTCCGCTT (reverse); GAPDH: TGTAGTTGAGGTCAATGAAGGG (forward), ACATCGCTCAGACACCATG (reverse). The thermocycling conditions were as follows. Initial activation stage: 95 °C for 30 s; two-step cycling stage: 95 °C for 5 s, and 60 °C for 30 s, 35–40 cycles.

2.4. Immunoblotting analysis

Cell pellets obtained by centrifugation were incubated with RIPA lysis buffer (Beyotime, China) and a proteinase inhibitor cocktail (Yeasen Biotechnology Co., Ltd., Shanghai, China) for 30 min on ice. Then, samples were incubated with deglycosylation enzymes (Endo-β1,4-galactosidase, Sigma-Aldrich, G6920) for 1 h at 25 °C to eliminate the effect of glycosylation modification on protein molecular weight [21]. The lysates were then centrifuged at 14,000 rpm for 10 min, and the supernatants were collected and stored at −80 °C. Lysate proteins were exposed to sodium dodecyl sulfate polyacrylamide gel electrophoresis (SDS-PAGE), transferred to a PVDF membrane, and subjected to immunoblotting following standard protocols. After blocking with 5% (w/v) nonfat milk for 1 h, the membranes were incubated with primary antibodies overnight at 4 °C. Primary antibodies used in immunoblotting analyses are listed in Table 1. The membranes were then incubated with the relevant HRP-conjugated secondary antibodies. Specific antibody-bound protein bands were visualized using Azure Biosystems C280 (Azure Biosystems, Inc., USA). Gray value was analyzed by Image-pro plus 6.0 (Media Cybernetics, Inc., Rockville, MD, USA). The relative protein expression is presented as the ratio of the gray value of the target bands to the GAPDH band.

2.5. Immunofluorescence (IF) analysis and cell transfection

IF analysis and cell transfection were performed according to our previous articles [22,23]. Specifically, cells were fixed in 4% (w/v) paraformaldehyde (Sangon Biotech, Shanghai, China) for 15 min and permeabilized with 0.5% (v/v) Triton X-100 (Thermo Fisher Scientific, Waltham, MA) for 5 min, followed by blocking with 5% (w/v) bull serum albumin (BSA; Yeasen Biotechnology Co., Ltd., Shanghai, China) for 1 h. The samples were incubated overnight at 4 °C with specific primary antibodies at the appropriate concentration and subsequently incubated with the fluorescent secondary antibody (Yeasen Biotechnology, China). CD63 (ab59479, Abcam, 1:200 dilution) and cytokeratin 1 (sc-65999, Santa Cruz Biotechnology, 1:200 dilution) were used for the immunofluorescence analysis. Cellular nuclei were counterstained with DAPI (Invitrogen, Thermo Fisher Scientific). All the labeled cells were examined

Table 1
Antibody.

Antibody	Manufacturer	Dilution rate
CD63	Abcam, ab59479	1:1000 for WB
	Santa Cruz, sc-5275	1:200 for IHC/ICC
		1:50 for TMA IHC
		1–2 μg per 100–500 μg of total protein for IP
KRT1	Santa Cruz, sc-65999	1:1000 for WB
		1:200 for IHC/ICC
		1–2 μg per 100–500 μg of total protein for IP
Vimentin	Abcam, ab92547	1:2000
Snail	CST, #3879	1:1000
β-catenin	CST, #9582	1:200
ZEB1	Abcam, ab203829	1:1000
E-cadherin	Abcam, ab40772	1:3000
Claudin-1	CST, #13255	1:1000
Ki-67	Abcam, ab16667	1:200
Cyclin B1	CST, #12231	1:1000
Cyclin A	CST, #4656	1:1000
Cyclin E2	CST, #4132	1:1000
P-Wee1(ser642)	CST, #4910	1:1000
P-Histone H3(ser10)	CST, #3377	1:1000
Myt1	CST, #4282	1:1000
p53	CST, #2527	1:1000
P-p53(ser15)	CST, #9286	1:1000
P21	CST, #2947	1:1000
GAPDH	Weiao, WB0197	1:2000

using microscope (Nikon inverted microscope ECLIPSE Ts2R, Japan). Fluorescence intensity was analyzed by Image-pro plus 6.0 (Media Cybernetics, Inc., Rockville, MD, USA) [22,23].

CD63 overexpression lentivirus (PGMLV-CMV-H_CD63-eGFP-3Flag-PGK-Blasticidin Lentivirus, Genomeditech, GM-6999LV) and/or shRNA-KRT1 (PGMLV-hU6-MCS-CMV-mScarlet-PGK-Puro Lentivirus, Genomeditech, GM-19167) were mixed with serum-free DMEM containing 10 μg/mL polybrene (Yeasen Biotechnology, China). The mixed solutions were added to the cells in logarithmic phase for another 12 h incubation before exchanging with fresh DMEM culture medium. After another 48 h incubation, 3 μg/mL blasticidin (Genomeditech, China) or 10ug/ml puromycin (Sigma, USA) was added to culture media for 1 week to select the stably transfected cells. Lentivirus particles based on corresponding empty vectors were used as controls [23].

2.6. Sphere formation assay

Suspension of 1×10^5 cells were planted on ultra-low adhesive 24-well plates (EFL, Suzhou) and cultured in serum-free medium, containing DMEM-F12 (HyClone, Logan, UT), 2% B-27™ supplement (ThermoFisher Scientific, Waltham, MA), 20 ng/mL animal-free recombinant human EGF, 20 ng/mL human FGF-basic (154 amino acids), 10 ng/mL human LIF (all from PeproTech, Rocky Hill, NJ) and 1% penicillin-streptomycin (Genom Biotechnology, China). Seven days after plantation, three fields of view in each well were randomly selected for imaging. The number of stem cell spheres was counted to assess sphere formation capacity.

2.7. Colony formation

A suspension of 1×10^3 cells was placed in each well of 6-well plates. When visible clones appeared in the well, the cells were fixed with 4% paraformaldehyde for 10 min, and then stained with 10% crystal violet for 10 min. The number of colonies was counted using Image-pro plus 6.0 (Media Cybernetics, Inc., Rockville, MD, USA).

2.8. EdU staining assays

To analyze cellular proliferation, EdU staining was conducted using the BeyoClick™ EdU Cell Proliferation Kit with Alexa Fluor 594 (Beyotime, Nantong, China). Briefly, the cells were incubated for 2 h at 37 °C/5% CO_2 with 10 μM EdU. After incubation, the cells were washed twice with PBS and then fixed in 4% paraformaldehyde at room temperature for 10 min before being stained with DAPI for 5 min. After washing, the stained cells were captured using inverted microscope (Nikon inverted microscope ECLIPSE Ts2R, Japan). The ratio of EdU-positive cells represents the proliferation ability of the cells.

2.9. Migration assay

Cells were maintained at 37 °C with 5% CO_2 in 24-well plates, and migration was monitored at 10-min intervals for 24 h using an inverted OLYMPUS LCS-IX81 microscope. Images were captured using a 10× air objective with a pixel size of 0.625 μm. Data were combined from time-lapse image series collected from at least three independent experiments. Individual cells migrating were tracked, and their trajectories were obtained using the FastTrack AI automated analysis system Chemotaxis (MetaVi Labs/Ibidi, Germany).

2.10. Cell cycle assay

Cells were starved for 24 h in serum-free culture medium to synchronize, then harvested during the logarithmic growth phase after another 12 h incubation. Single-cell suspensions were then fixed in 75% pre-cooling ethanol overnight at −20 °C, washed twice with pre-cooling PBS, and then incubated with 500 μL PI/RNase staining buffer (BD Biosciences) for 15 min in dark. After filtering with a 40 μm mesh screen (BD Biosciences), cells were then tested using flow cytometry (SP8 MoFlo XDP, Beckman Coulter), and the cell cycle distribution was investigated with FlowJo Software (FlowJo LLC).

2.11. Immunoprecipitation (IP)

Cells were lysed with 1000 μL ice-cold IP lysis buffer (Beyotime, Nantong, China) on ice for 30 min with periodic mixing. We then transferred the lysate to a microcentrifuge tube, which was centrifuged at 12,000 rpm for 15 min to pellet the cell debris at 4 °C. Protein A/G Magnetic Beads and Magnet Starter Pack (Thermo Scientific) were used to immunoprecipitate the magnetic beads-Ab-Ag complex, following the manufacturer's protocol. Mouse lgG (sc-2025, Santa Cruz Biotechnology) was used as a control. The proteins were separated by electrophoresis, and the binding protein was detected by immunoblotting analysis or liquid chromatography-tandem mass spectrometry (LC-MS/MS).

2.12. Mass spectrometry and co-immunoprecipitation assays (Co-IP)

LC-MS/MS was performed using an EASY-nLC™ ab00 UHPLC system (Thermo Fisher) coupled with a Q Exactive HF mass spectrometer (Thermo Fisher) with the assistance of Shanghai Lu Ming Biotech Co., Ltd. (Shanghai, China). The Co-IP assay was carried out using a co-immunoprecipitation Kit (Millipore, Billerica, MD, USA) following the manufacturer's protocols. In brief, the cells were harvested and lysed and then incubated with IgG or specific for CD63 (sc-5275, Santa Cruz Biotechnology)/KRT1 antibody (sc-65999,

Santa Cruz Biotechnology) rotated at 4 °C overnight. Bead-bound proteins were released and analyzed by immunoblotting analysis.

2.13. Molecular docking

Protein structure was obtained by Swiss-Model (https://swissmodel.expasy.org/). All protein structures are processed in the molecular operating environment (MOE 2019.1) platform, including removal of water and ions, protonation, addition of missing atoms, complementing missing groups, and minimizing protein energy. Using HDOCK software, set the protein to rigid, the docking contact site to the full surface, the conformation generated after docking is set to 100, and the scoring function is used to select the conformation with the most negative energy.

2.14. Gene set enrichment analysis (GSEA)

GSEA was performed to elucidate KRT1-related pathways and gene sets in HNSCC. The gene expression profiles of 497 HNSCC samples were downloaded from the Cancer Genome Atlas (TCGA) datasets. According to KRT1 expression, the first 50% and last 50% samples were divided into high- and low-KRT1 groups, respectively. The number of permutations was 1000, and the threshold for the adjusted p-value was set to 0.05. A gene set is considered to be associated with KRT1 if most of its members are positively or negatively

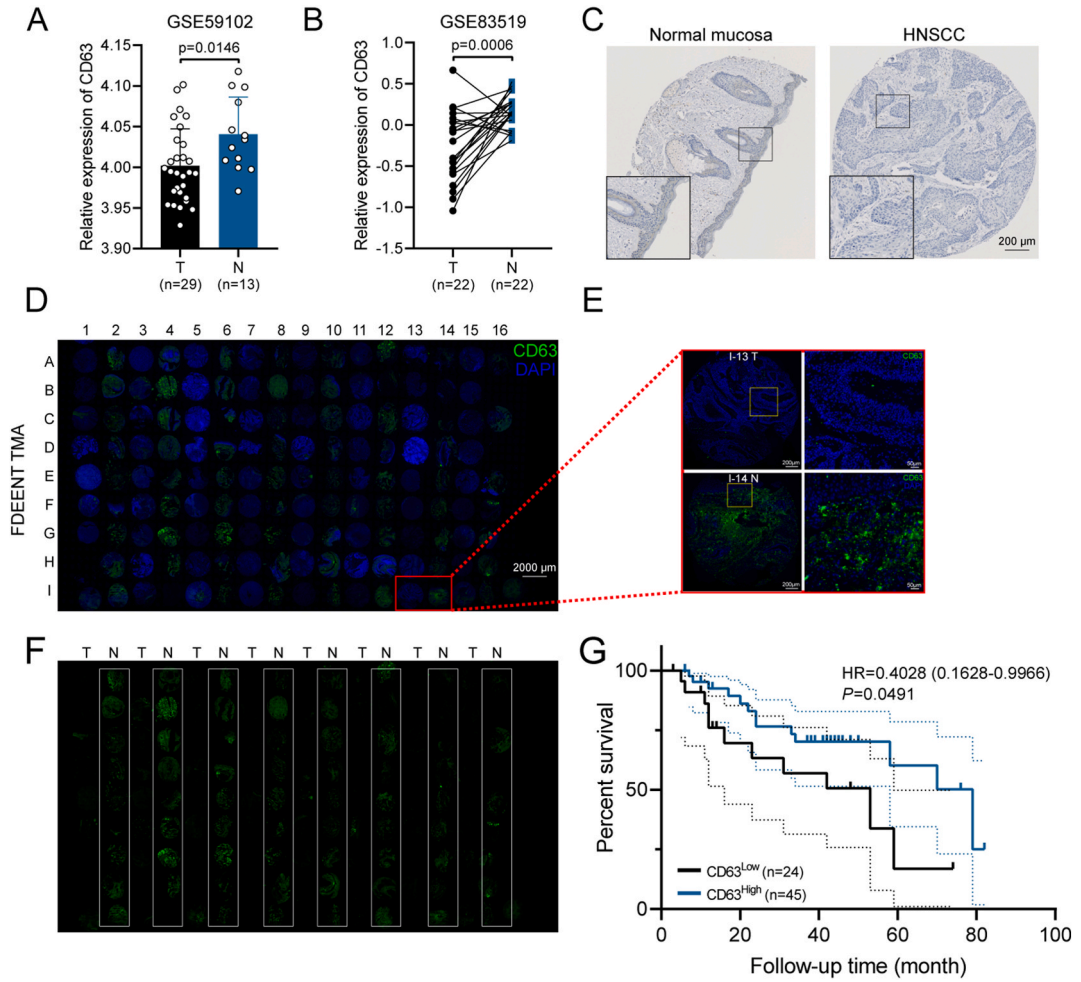

Fig. 1. CD63 is downregulated in HNSCC tissue and is correlated with prognosis. (A) CD63 mRNA expression levels were analyzed in HNSCC (T, Tumor, n = 29) and normal epithelial tissue (N, Non-tumor, n = 13) in the GSE59102 database. **(B)** CD63 mRNA expression levels were analyzed in paired HNSCC and adjacent tissue (n = 22) in the GSE83519 database. **(C)** Representative IHC staining image of CD63 in commercial TMA. Magnified images from the regions marked by rectangles were showed in the bottom. Scale bar, 200 μm. **(D)** General observation of CD63 immunofluorescence staining in TMA among 69 HNSCC patients from our center. Scale bar, 2000 μm. **(E)** Partially amplified images are shown in the frame. Scale bar, 50 μm; CD63, green; DAPI, blue. **(F)** General observation of the difference between tumor and adjacent tissue. White rectangles, adjacent tissue. **(G)** Kaplan–Meier analysis of overall survival in patients with different CD63 expression subgroups. (For interpretation of the references to color in this figure legend, the reader is referred to the Web version of this article.)

correlated with KRT1.

2.15. In vivo metastasis assay

For the *in vivo* metastasis assay, we injected 1×10^6 cell suspensions in 200 μL PBS into the tail vein in each group of 6-week-old male nude mice with a 29 G syringe needle and observed the survival of mice daily to obtain a survival curve. Eighty days post-injection, all mice that had not yet died were euthanized, and the lungs were dissected for subsequent histological assessment. A successful lung metastasis model is defined as one in which metastatic nodules are clearly seen on the surface of lung tissue upon pathological examination, or in which tumor tissue is found on lung tissue slices after HE staining.

2.16. Immunohistochemical analysis (IHC)

IHC analysis was performed as previously described [22], with a slight modification. The tumor tissue excised from nude mice and patient specimens were fixed, dehydrated, and embedded in paraffin. Paraffin blocks were then sliced into 4-μm sections and subjected to IHC, followed by 30 min of incubation with biotin-labeled secondary antibody. The positive number and staining intensity in each section were converted into corresponding H-score values to achieve semi-quantitative tissue staining. H-Score = $\sum$(pi × i) = (percentage of weak intensity area × 1) + (percentage of moderate intensity area × 2) + (percentage of strong intensity area × 3), where *pi* represents the percentage of pixel area of positive signal; *i* for positive grade. The quantitative calculation process was completed by IHC Profiler plug-in in ImageJ software [24].

2.17. Microarray datasets

To verify the expression of CD63, microarray datasets GSE59102 (derived from the GPL6480 platform) and GSE83519 (derived from the GPL4133 platform) were selected from the GEO database (http://www.ncbi.nlm.nih.gov/geo). We downloaded the series matrix files and platform files. Each gene probe ID in the matrix files was converted to the gene symbol in the platform files by Perl. The

Table 2
Correlation between CD63 staining and clinicopathologic characteristics in 69 HNSCC patients.

	Cases	CD63 (relative fluorescence intensity)	*t*-test	*P value*
Age				
≤60	26	0.025 ± 0.020	0.518	0.607
>60	43	0.027 ± 0.023		
Smoke				
Smoke	53	0.027 ± 0.023	0.118	0.907
Non-smoke	16	0.026 ± 0.020		
Drink				
Drink	33	0.025 ± 0.021	0.462	0.646
Non-drink	36	0.028 ± 0.023		
Hypertension				
No	49	0.028 ± 0.023	1.402	0.167
Yes	20	0.021 ± 0.017		
Diabetes				
No	59	0.025 ± 0.021	0.935	0.37
Yes	10	0.034 ± 0.028		
Stage[a]				
I-II	11	0.028 ± 0.026	0.285	0.781
III-IV	58	0.026 ± 0.021		
T stage				
T1-2	19	0.022 ± 0.022	1.ab9	0.267
T3-4	50	0.028 ± 0.022		
N stage				
N0	**37**	**0.031 ± 0.024**	**2.083**	**0.041**
N1+	**32**	**0.021 ± 0.017**		
Location				
Non-glottic	39	0.023 ± 0.020	1.45	0.153
glottic	30	0.031 ± 0.024		
Differentiation				
Moderately + poorly	59	0.026 ± 0.021	0.165	0.872
Well + moderately	10	0.028 ± 0.028		
Tumor size				
≤3 cm	26	0.028 ± 0.022	0.469	0.642
> 3 cm	43	0.025 ± 0.022		
Recurrence				
Yes	30	0.026 ± 0.021	0.179	0.859
No	39	0.027 ± 0.023		

[a] According to the 8th American Joint Committee on cancer (AJCC) stage system.

expression of CD63 in each dataset was then extracted and calculated.

2.18. Statistical analysis

In each case, the data were pooled and averaged, and the standard deviation (SD) was calculated using GraphPad Prism (version 8; GraphPad Software, La Jolla, CA). Figure legends specify the *n* and error bars for each experiment. Student's t-test or one-way ANOVA was performed to evaluate the differences between two groups or more than two groups. Spearman's correlation was performed to analyze the correlation of gene expression. Differences were considered significant if the P value was <0.05 (*), <0.01(**), <0.001 (***), or <0.0001 (****), as indicated in each figure legend.

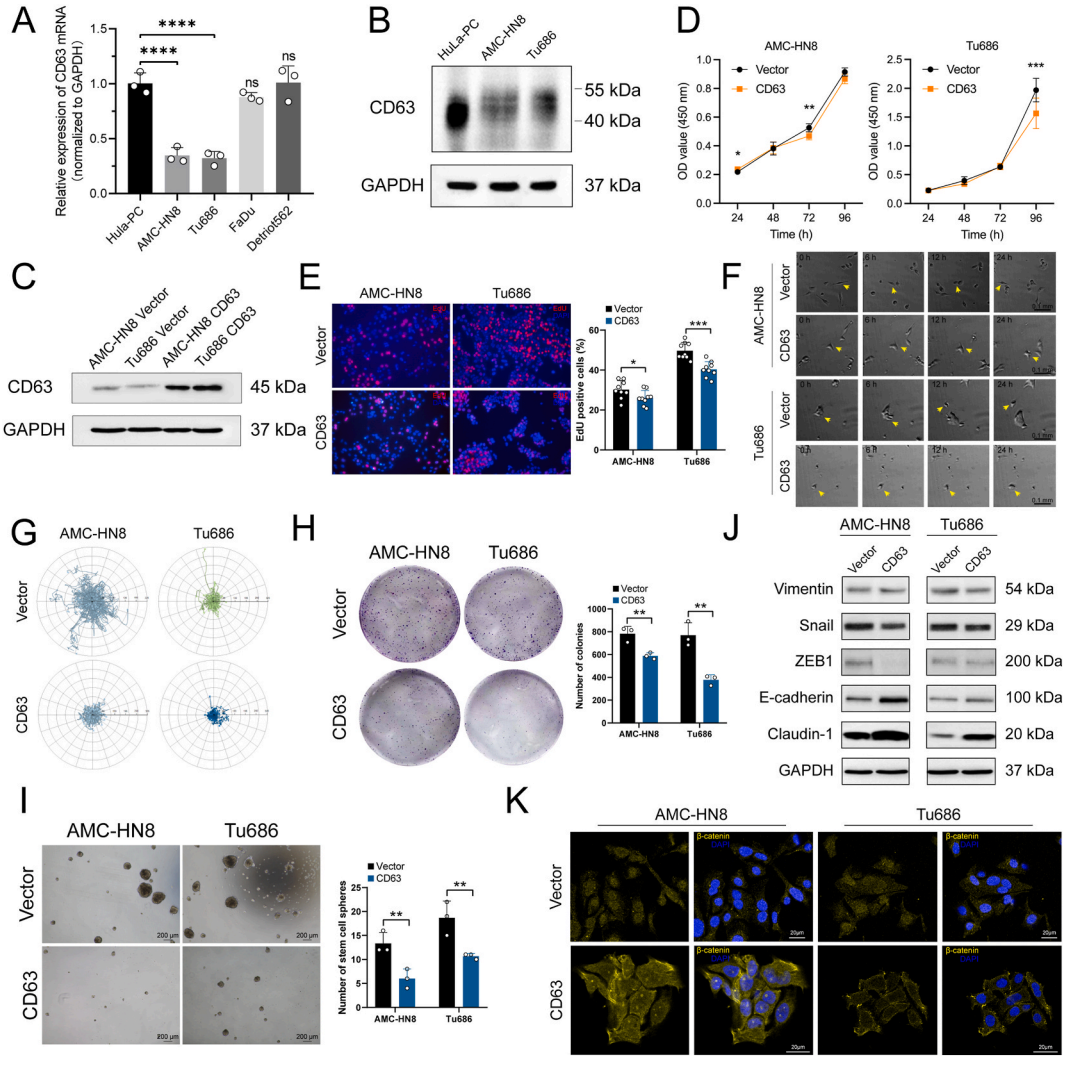

Fig. 2. CD63 inhibits the proliferation, migration, stemness, and EMT of HNSCC cells in vitro. (A–B) CD63 expression in HNSCC cell lines (AMC-HN8, Tu686, FaDu, and Detroit562) compared with that in the normal epithelial cell line HuLa-PC detected by qRT-PCR and western blotting. Lentiviral vectors that overexpressed CD63 in established HNSCC cell lines, AMC-HN8 and Tu686 cells was conducted **(C)**. Cell proliferation assays **(D)**, EdU assays **(E)**, cell migration **(F-G)**, colony formation assays **(H),** and sphere formation capacity **(I)** in the vector group and CD63-overexpressed AMC-HN8 and Tu686 cell groups. **(F)** Representative images of each particular point in time in living cell imaging. The time span was 24 h. Scale bar, 0.1 mm. Yellow arrows, migrating cells. **(G)** Data were combined from time-lapse image series collected from at least three independent experiments. Individual cells migrating were tracked, and their trajectories were obtained using the FastTrack AI automated analysis system. **(J)** Western blot validation of EMT-related protein expression in the vector group and CD63-overexpressed group. **(K)** Representative images of the immunofluorescence analysis of β-catenin. Scale bar, 20 μm. All data are shown as mean ± SD. *, $P < 0.05$; **, $P < 0.01$; ***, $P < 0.001$, ****, $P < 0.0001$. (For interpretation of the references to color in this figure legend, the reader is referred to the Web version of this article.)

3. Results

3.1. CD63 is downregulated in HNSCC tissue and is correlated with prognosis

To explore the expression of CD63 in HNSCC tissue, the GSE59102 and GSE83519 datasets were obtained from the GEO database and comprehensively analyzed, revealing that CD63 was significantly downregulated in HNSCC tumor tissue compared with normal tissue (Fig. 1A and B). To verify this result, we performed TMA IHC staining, founding that CD63 is positive in the normal mucosa, but not in HNSCC tissue. (Fig. 1C, Supplementary Fig. 1). Further, Using 69 pairs of postoperative specimens from our cohort (FDEENT TMA), we validated that CD63 expression was downregulated in HNSCC tissue compared with adjacent tissue (Fig. 1D–F), consistent with the GEO database and commercial TMA. We conducted a Kaplan–Meier survival analysis of 69 patients from our cohort. The results revealed that CD63 expression was positively associated with overall survival (OS) (Fig. 1G). We then analyzed the correlation between CD63 and the clinical data. CD63 expression was significantly associated with lymph node metastasis ($p = 0.041$) (Table 2). However, no correlation was observed between CD63 and clinical stage, tumor location, pathological differentiation, or recurrence. CD63 expression was also downregulated in two established HNSCC cell lines (AMC-HN8 and Tu686) compared with HuLa-PC, a human epithelial cell from the posterior commissure of the larynx (Fig. 2A and B). These results showed that CD63 was significantly reduced in HNSCC tissue and is associated with prognosis and metastasis.

3.2. CD63 inhibits the proliferation, migration, stemness, and EMT of HNSCC cells in vitro

We then characterized the phenotype landscape to fully demonstrate the function of CD63 in HNSCC *in vitro*. We designed and constructed lentiviral vectors that overexpressed CD63 in established HNSCC cell lines, AMC-HN8 and Tu686 cells (Fig. 2C). CCK8 proliferation assay, EdU staining assay, sphere formation assay, cell migration assays, and colony formation assays were performed to measure the effect of CD63 on HNSCC cell proliferation and migration. We found that overexpression of CD63 significantly impaired the proliferation and migration properties of HNSCC cells (Fig. 2D–I). We assessed the effect of CD63 on EMT via western blotting, which demonstrated that overexpression of CD63 significantly decreased the expression of Vimentin, Snail, and ZEB1, but dramatically enhanced the expression of E-cadherin and Claudin-1 (Fig. 2J). This conclusion was further confirmed by confocal laser microscopy observation that the overexpression of CD63 disrupted the accumulation of β-catenin translocation from cytoplasm to nucleus, which is a key effector of EMT (Fig. 2K).

3.3. CD63 reduces lung metastasis in vivo

To investigate the role of CD63 in tumor metastasis *in vivo*, a lung metastasis model was established. We injected different subgroups of HNSCC cells into nude mice via the tail vein and observed the survival of mice daily to obtain a survival curve. After 80 days, we found that tumor cells preferentially colonize the lungs in this transplant model, and the tumor-bearing mice in the CD63 overexpression subgroup had a better overall survival rate ($p = 0.0221$ for AMC-HN8 cells, $p = 0.0293$ for Tu686 cells) (Fig. 3A). The

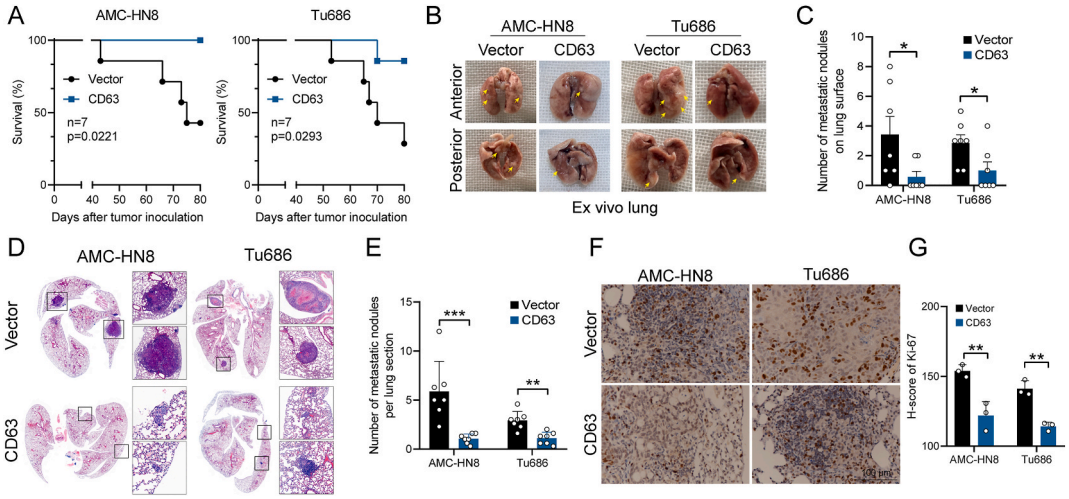

Fig. 3. CD63 reduces lung metastasis *in vivo*. (A) Kaplan–Meier analysis of overall survival in tumor-bearing mice with different CD63 expression subgroups. Mice were transplanted with vector or CD63-overexpressed cells by tail vein injection (n = 7/group). **(B–C)** Representative images from each group were taken to observe and calculate the number of metastatic nodules on the lung surface. **(D)** H&E staining of lung sections. **(E)** The number of pulmonary metastases was counted or measured in random microscopic fields of each lung section. **(F)** Immunohistochemical staining was used to detect Ki-67 expression in pulmonary metastases tissue (n = 3). Scale bar, 100 μm. **(G)** Quantitative analysis of H-scores of Ki-67. All data are shown as mean ± SD. *, $P < 0.05$; **, $P < 0.01$; ***, $P < 0.001$.

number and incident rate of metastatic nodules on the lung surface drastically decreased with CD63 overexpressed cells compared to the control cells (Fig. 3B and C).

The presence of pulmonary metastatic nodules of dissected lung tissue was also tested using H&E staining. There was an obvious reduction in the number of tumors per section in the CD63 overexpression subgroup (Fig. 3D and E). We also found that Ki-67 expression was lower in pulmonary metastases nodules tissue of the CD63 overexpressed subgroup (Fig. 3F and G). These data provide evidence that CD63 is involved in reducing HNSCC cell metastasis *in vivo*.

3.4. KRT1 is a direct interacting partner of CD63

To investigate the molecular mechanism underlying CD63-mediated suppression of HNSCC progression, we identified CD63-interacting proteins using mass spectrometry-based methods and co-localization image analysis. CD63 binding candidates were recognized by bands that were specifically found in CD63-overexpressing cells (Fig. 4A). We found that KRT1, also known as keratin 1, was one of the prominent proteins in the eluent via mass spectrometry. To confirm the interaction of CD63 with KRT1, co-immunoprecipitation was performed. As expected, a positive KRT1 signal was observed in the immunoprecipitate pulled down using the anti-CD63 antibody. Reciprocal co-immunoprecipitation by anti-KRT1 antibody also resulted in the detection of CD63 (Fig. 4B). The overexpression of CD63 in the cells was accompanied by increased KRT1 expression (Fig. 4C). Furthermore, confocal microscopy showed that CD63 and KRT1 were co-localized in the cytomembrane of HNSCC cells (partly present in the cytoplasm in Tu686 cells) (Fig. 4D). Molecular docking predicted that the binding score of CD63 and the KRT1 protein was −301.96 kcal/mol (Table 3). The binding sites of CD63 protein include LEU-92, SER-91, THR-85, CYS-81, and other amino acid residues. The binding sites of KRT1 include TYR-206, ARG-192, ARG-178, and other amino acid residues. Thus, CD63 and KRT1 contact residues can form a variety of interactions, such as salt bridges, hydrogen bonds, hydrophobic interactions, and other interactions. These interaction forces can effectively improve the stability of the CD63 and KRT1 protein complexes (Fig. 4E–G). These results imply direct physical interaction and co-localization of CD63 and KRT1 in HNSCCC cells.

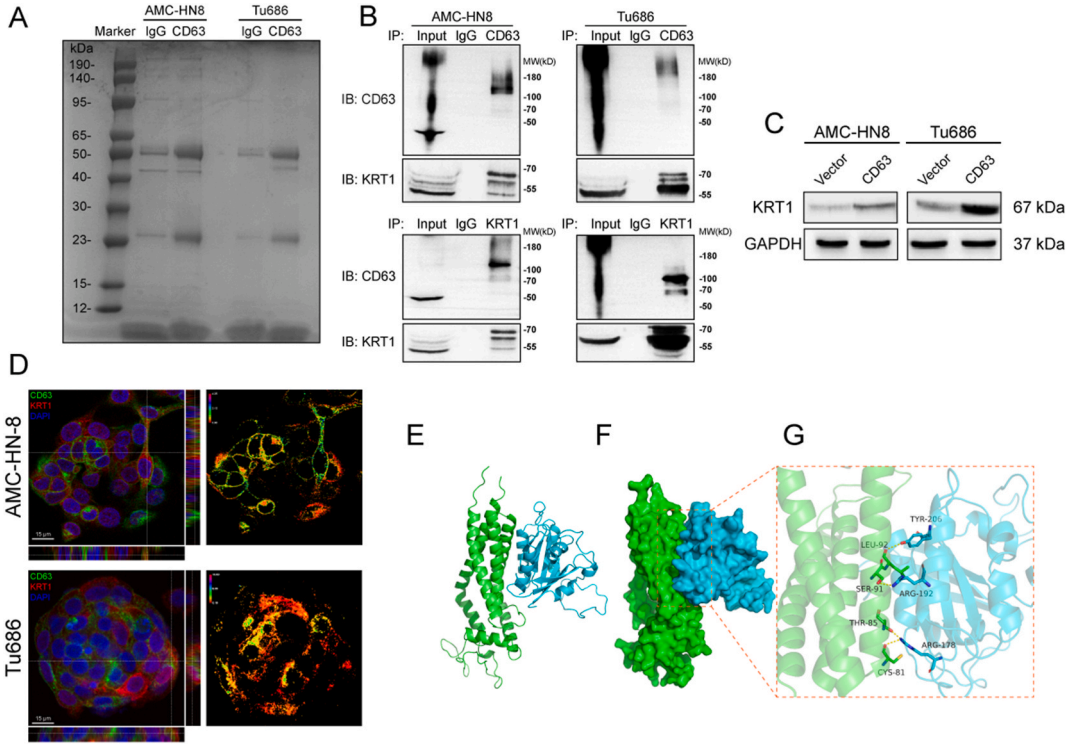

Fig. 4. KRT1 is a direct interacting partner of CD63. (A) Coomassie blue staining of the immunoprecipitation pellet. **(B)** Co-IP assays of the CD63–KRT1 interaction. Cell lysates were precipitated (IP) with anti-CD63 antibody, and the precipitates were blotted (IB) with anti-KRT1 antibody (top). Conversely, cell lysate was precipitated with anti-KRT1 antibody and blotted with anti-CD63 antibody (bottom). Non-IP cell lysates (10%) were used as input controls. **(C)** Western blot analysis of KRT1 in the vector and CD63-overexpressed cells. **(D)** Representative orthogonal view of the immunofluorescence analysis of CD63 (green) and KRT1 (red) in the cells. Fluorescence ratio image (right panel) indicated colocalization and located in the region where CD63 and KRT1 interact. **(E–G)** Molecular modeling of a putative interaction between CD63 and KRT1. **(E)** The backbone of the protein was rendered in tube form and colored. **(F)** The electrostatic surfaces of CD63 (left) and KRT1 (right) proteins. **(G)** Detailed binding mode of CD63 with KRT1. The yellow dash represents a hydrogen bond or salt bridge. (For interpretation of the references to color in this figure legend, the reader is referred to the Web version of this article.)

Table 3
The docking results of two target protein.

Protein1	Protein2	Binding Energy (kcal/mol)	Contact Sites (protein1)	Contact Sites (protein2)	Combination Type
CD63	KRT1	−301.96	LEU-92, SER-91, THR-85, CYS-81	TYR-206, ARG-192, ARG-178	Salt bridge, Hydrogen bond, Hydrophobic interaction

3.5. CD63 reduces HNSCC progression via KRT1-mediated cell cycle arrest

We found a significant relationship between cell cycle-related genes, especially p53 and KRT1, in HNSCC using GSEA (Fig. 5A). Therefore, we used vitro models to explore the effects of silencing KRT1 on HSNCC cell cycle regulation. We found that the depletion of KRT1 altered cell cycle-associated genes and reduced the proportion of cells in the S phase of the cell cycle (Fig. 5B–D), indicating that KRT1 functionally arrests the cell cycle of HNSCC. Subsequently, we found that overexpression of CD63 increased the proportion of

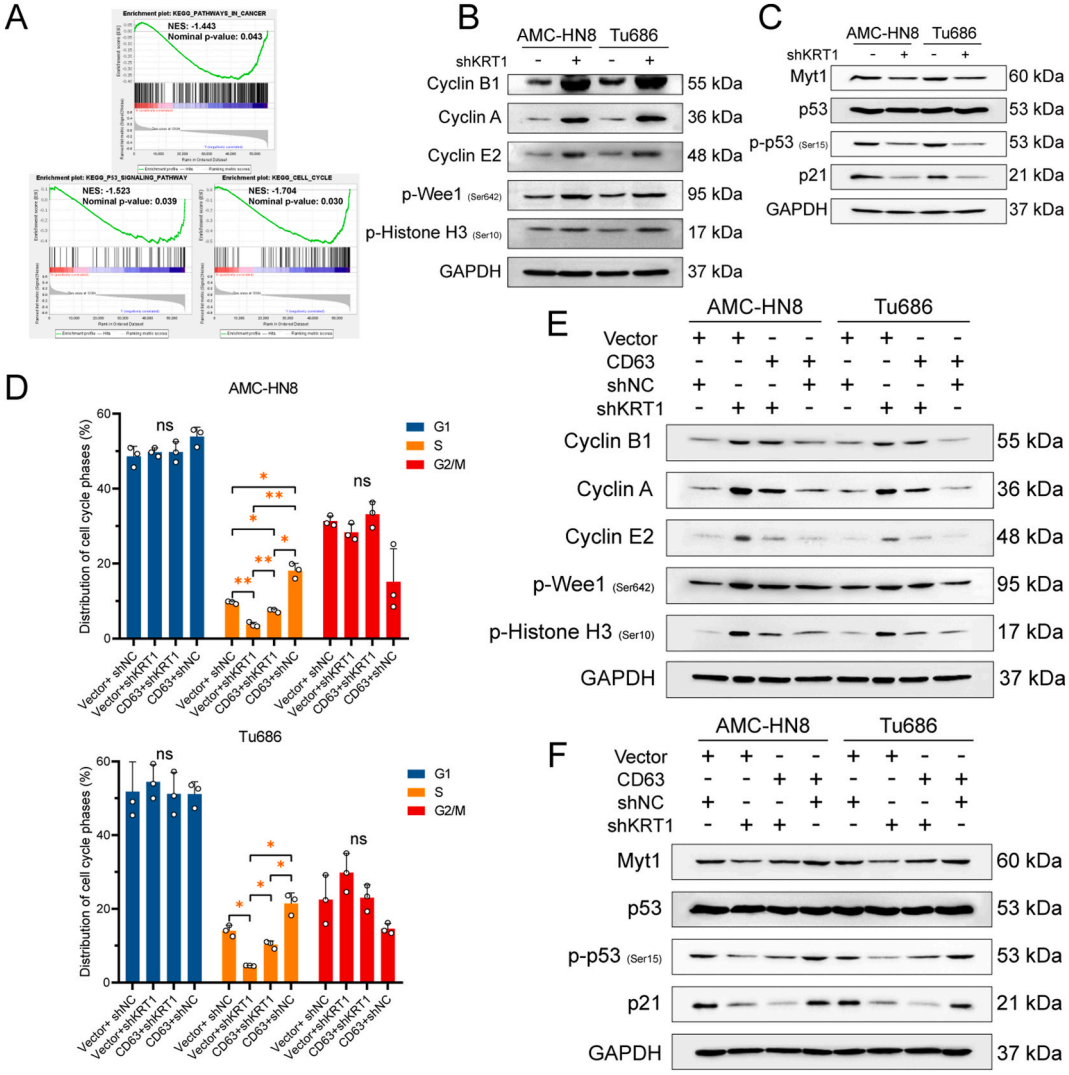

Fig. 5. KRT1 arrests the HNSCC cell cycle by mediating p53 *in vitro*. (A) The GSEA results were plotted to visualize the correlation between the expression of KRT1 and dysregulated genes associated with the cell cycle and the p53 signaling pathway in HNSCC. **(B–C)** The protein levels of cell cycle regulation-related genes were detected by western blotting after KRT1 silencing. **(D)** Cell cycle assay was performed to show the properties of cell cycle regulation in the indicated subgroups. **(E–F)** The protein levels of cell cycle regulation-related genes were detected by western blotting in the indicated subgroups. All data are shown as mean ± SD. *, $P < 0.05$; **, $P < 0.01$.

cells in the S phase of the cell cycle, thereby blocking cell cycle progression, while simultaneous KRT1 depletion in cells overexpressing CD63 mitigated this effect (Fig. 5D and E). These data prove that CD63 reduces HNSCC progression via KRT1-mediated cell cycle arrest.

3.6. The clinical relevance of CD63 and KRT1 in HNSCC

To examine the clinical impact of CD63 and KRT1 on HNSCC, we analyzed CD63 and KRT1 expression in paired tumors and adjacent normal (n = 124) tissue samples isolated from HNSCC patients. We found that the expression of CD63 and KRT1 in normal adjacent tissue was significantly higher than in paired tumor tissue (Fig. 6A and B). The correlation analysis indicated a positive correlation between CD63 and KRT1 mRNA expression, suggesting that both proteins had the same inhibitory effect on HNSCC (Fig. 6C). Furthermore, we verified these results by immunoblotting analysis of fresh paired pathological tissue (n = 16) (Fig. 6D and E).

Moreover, to detect the expression of CD63 and KRT1 in primary and metastatic HNSCC tissue, we collected and tested tissue derived from the primary tumor region and cervical lymph node metastasis region (n = 13). As expected, we found that CD63 and KRT1 expression were significantly decreased in the metastatic region. These results suggest that CD63 and KRT1 reduce the metastasis of HNSCC (Fig. 6F–I).

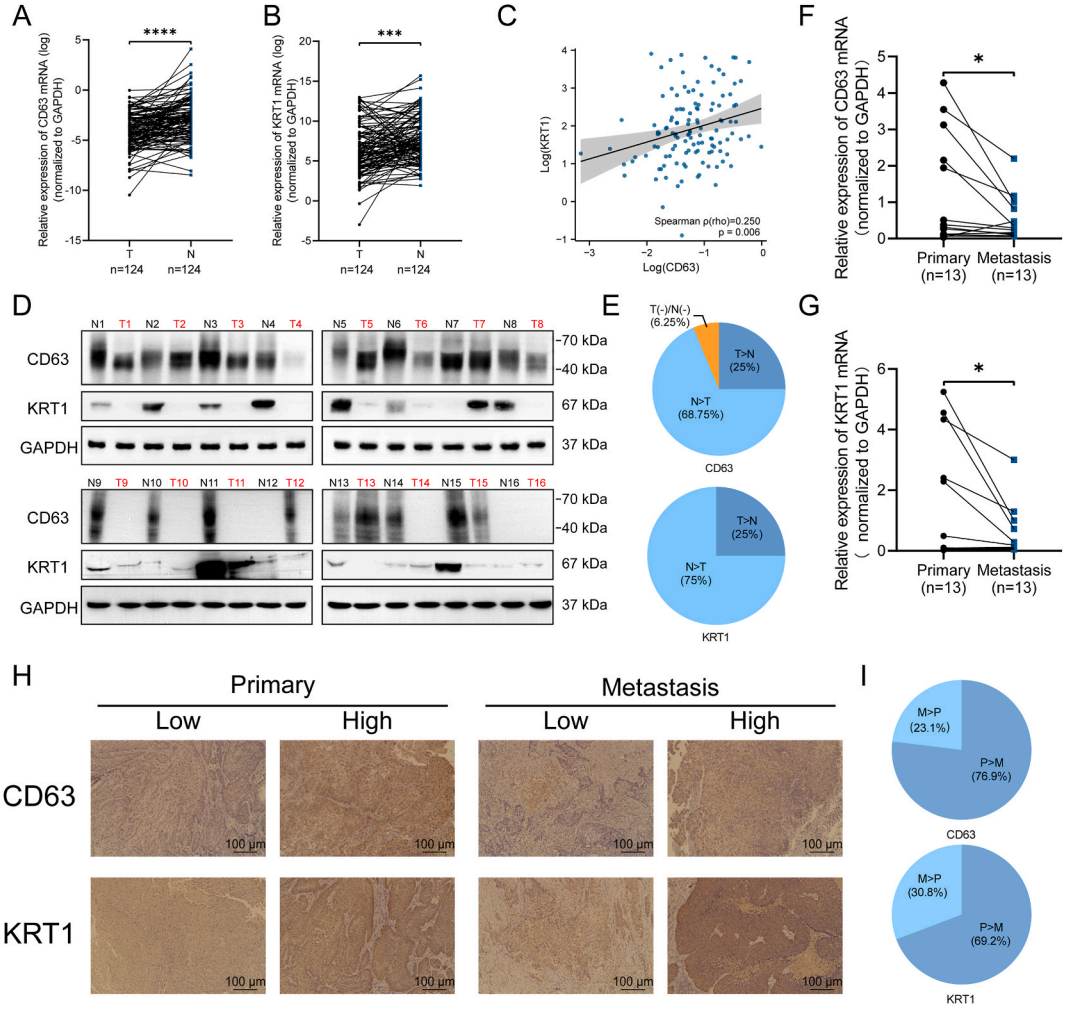

Fig. 6. The clinical relevance of CD63 and KRT1 in HNSCC. **(A–B)** Comparison of CD63 and KRT1 expression in paired HNSCC tumor tissue and adjacent normal tissue by qRT-PCR (n = 124). **(C)** The correlation analysis indicated a positive correlation between CD63 and KRT1 expression. **(D)** Western blot analysis of CD63 and KRT1 protein expression in paired HNSCC tumor tissue and adjacent normal tissue (n = 16). **(E)** Quantitative calculation and statistics of the gray value. **(F–G)** Comparison of CD63 and KRT1 expression in paired primary HNSCC tumor tissue and cervical lymph node metastasis tissue by qRT-PCR (n = 13). **(H)** Representative images of immunohistochemical analysis of CD63 and KRT1 in paired primary HNSCC tumor tissue (P) and cervical lymph node metastasis tissue (M). Scale bar, 100 μm. **(I)** Quantitative calculation and statistics of the H-score. *, $P < 0.05$; ***, $P < 0.001$, ****, $P < 0.0001$.

4. Discussion

In this study, we indicated that CD63 reduced the metastatic potential of HNSCC cells by regulating KRT1-mediated cell cycle arrest. Our findings show that the expression of CD63 had an impact on the intrinsic metastatic potential of HNSCC cells, as overexpression of CD63 produced decreased metastases. These observations support the notion of an anti-metastatic role of CD63 [25], which is also in line with clinical studies showing that CD63 is downregulated in tumor cells of cancer patients [26,27].

Our findings are in contrast to earlier reports suggesting a tumor-stimulative role of CD63, which studied the effect of CD63 in breast cancer cells [28] and other tumor cells [18]. Previous studies have indicated that CD63 might differ in its role during other stages of cancer progression, or it may play completely different or even opposite roles in various tumors [12,29,30]. CD63 is reportedly a highly N-glycosylated type III lysosomal membrane protein [31,32], and its glycosylation status may have a great influence on its role in tumor cells [28].

Although the predicted molecular weight of CD63 is 25 kDa [33], we found that the molecular weight of endogenous CD63 was 40–55 kDa (Fig. 2B), while the molecular weight of CD63 of two HNSCC cells after CD63 overexpression shifted to 55–100 kDa (Fig. 4C). Although the alteration between predicted and actual molecular weight can be explained by glycosylation modification [9], the mechanism underlying the difference in molecular weight before and after the overexpression of CD63 still needs more research.

It is known that tetraspanin CD63 regulates cellular invasiveness through its association with peptidases and interacting proteins [7,8]. Jung et al. identified CD63 as a cell-surface binding partner of TIMP-1, regulating TIMP-1-driven cell survival and polarization by modulating the tetraspanin/integrin signaling complex [34]. In the present study, we identified KRT1 as the direct interacting partner of CD63 in HNSCC cells through co-localization studies, an hitherto unknown interaction. Similar to our finding, Suárez observed that CD63 polypeptide treatment changed the expression of KRT1, but no in-depth mechanistic studies were further conducted to explain this change [35]. Keratins, especially KRT1, the intermediate filament-forming proteins of epithelial cells [36], are extensively used as diagnostic biomarkers in cancers and are associated with tumorigenesis and metastasis in multiple cancers [37,38]. We found that KRT1, together with CD63, is prominently decreased in metastatic tissue compared with primary tumor tissue, which is consistent with findings in melanoma [39].

The research in this article has some limitations. First, the key gene of this study, CD63, was not selected through systematic screening, with the consequence that other, more critical genes that may be responsible for HNSCC metastasis were not studied. Second, though we revealed a previously unrecognized role of CD63 in regulating KRT1-mediated cell cycle arrest in HNSCC cells, we have not conducted experiments to investigate the role of epigenetics in CD63-mediated cell cycle arrest. This makes the content of the article not perfect and in-depth.

To our knowledge, we believe that this is the first work to disclose a previously unrecognized role of CD63 in regulating KRT1-mediated cell cycle arrest in HNSCC cells, and our findings contribute to defining an important mechanism of HNSCC progression and metastasis.

Ethics approval and consent to participate

The current study was approved by the Ethics Committee of the Eye & ENT Hospital of Fudan University (NO.KJ2008–01) and performed in strict accordance with the Declaration of Helsinki. All participants in this study signed informed consent documentation before sample collection. Animal experiments were approved by the Ethics Committee of the Eye & ENT Hospital of Fudan University and strictly performed according to the Guide for the Care and Use of Laboratory Animals published by the US National Institutes of Health. Due efforts were made to limit animals' pain.

Author contribution statement

Qiang Huang; Yu-Jie Shen; Chi-Yao Hsueh; Yi-Fan Zhang: Conceived and designed the experiments; Performed the experiments; Analyzed and interpreted the data; Contributed reagents, materials, analysis tools or data; Wrote the paper.

Yang Guo; Xiao-Hui Yuan; Chun-Yan Hu; Jiao-Yu Li; Lei Tao: Performed the experiments.

Hong-Li Gong; Ming Zhang; Liang Zhou: Conceived and designed the experiments; Wrote the paper.

Data availability statement

Data will be made available on request.

Funding

The present study was supported by grants from the National Natural Science Foundation of China [No. 81972529; 81502343], the Science and Technology Commission of Shanghai Municipality [No. 19411961300; 21Y11900100], Shanghai "Rising Stars of Medical Talent" Youth Development Program-Specialist Program [No. 2019–72], Shanghai Sailing Program [No. 21YF1405600; 22YF1405700; 23YF1404700], and Clinical Research Plan of SHDC [No. SHDC2020CR6011].

Declaration of competing interest

The authors declare that they have no known competing financial interests or personal relationships that could have appeared to influence the work reported in this paper.

Appendix A. Supplementary data

Supplementary data to this article can be found online at https://doi.org/10.1016/j.heliyon.2023.e17711.

References

[1] R.L. Siegel, K.D. Miller, A. Jemal, Cancer statistics, 2020, CA A Cancer J. Clin. 70 (2020) 7–30.
[2] F. Bray, J. Ferlay, I. Soerjomataram, R.L. Siegel, L.A. Torre, A. Jemal, Global cancer statistics 2018: GLOBOCAN estimates of incidence and mortality worldwide for 36 cancers in 185 countries: global cancer statistics 2018 [Internet], CA: Canc. J. Clin. (2018), https://doi.org/10.3322/caac.21492 [cited 2018 Sep 15]; . Available from:.
[3] C. Hu, Q. Huang, Q. Sun, The regulation of lymph node pre-metastatic niche formation in head and neck squamous cell carcinoma, Front. Oncol. 12 (2022), 852611.
[4] Chow LQM. Head and neck cancer, N. Engl. J. Med. 382 (2020) 60–72.
[5] S.-C. Yang, W.-Y. Wang, J.-J. Zhou, L. Wu, M.-J. Zhang, Q.-C. Yang, W.-W. Deng, Z.-J. Sun, Inhibition of DNMT1 potentiates antitumor immunity in oral squamous cell carcinoma, Int. Immunopharm. 111 (2022), 109113.
[6] D. Tang, D. Zhang, Y. Heng, X.-K. Zhu, H.-Q. Lin, J. Zhou, L. Tao, L.-M. Lu, Tumor-infiltrating PD-l1+ neutrophils induced by GM-CSF suppress T cell function in laryngeal squamous cell carcinoma and predict unfavorable prognosis, J. Inflamm. Res. 15 (2022) 1079–1097.
[7] M.S. Pols, J. Klumperman, Trafficking and Function of the Tetraspanin CD63, Experimental Cell Research, 2009, p. 9.
[8] M.E. Hemler, Tetraspanin functions and associated microdomains, Nat. Rev. Mol. Cell Biol. 6 (2005) 801–811.
[9] A. Lupia, S. Peppicelli, E. Witort, F. Bianchini, V. Carloni, N. Pimpinelli, C. Urso, L. Borgognoni, S. Capaccioli, L. Calorini, M. Lulli, CD63 tetraspanin is a negative driver of epithelial-to-mesenchymal transition in human melanoma cells, J. Invest. Dermatol. 134 (2014) 2947–2956.
[10] S.N. Hurwitz, M.R. Cheerathodi, D. Nkosi, S.B. York, D.G. Meckes, Tetraspanin CD63 bridges autophagic and endosomal processes to regulate exosomal secretion and intracellular signaling of epstein-Barr Virus LMP1. Longnecker RM [Internet], J.Virol. (2017) [cited 2020 Feb 11]; 92. Available from: http://jvi.asm.org/lookup/doi/10.1128/JVI.01969-17.
[11] S.N. Hurwitz, D. Nkosi, M.M. Conlon, S.B. York, X. Liu, D.C. Tremblay, D.G. Meckes, CD63 regulates epstein-Barr Virus LMP1 exosomal packaging, enhancement of vesicle production, and noncanonical NF-κB signaling. Longnecker RM, editor [Internet], J. Virol. (2017) [cited 2018 Aug 18]; 91. Available from: http://jvi.asm.org/lookup/doi/10.1128/JVI.02251-16.
[12] K.J. Radford, R.F. Thorne, P. Hersey, Regulation of tumor cell motility and migration by CD63 in a human melanoma cell line, J. Immunol. 158 (1997) 3353–3358. United States.
[13] H. Hotta, A.H. Ross, K. Huebner, M. Isobe, S. Wendeborn, M.V. Chao, R.P. Ricciardi, Y. Tsujimoto, C.M. Croce, H. Koprowski, Molecular cloning and characterization of an antigen associated with early stages of melanoma tumor progression, Canc. Res. United States 48 (1988) 2955–2962. United States.
[14] B. Atkinson, C.S. Ernst, B.F. Ghrist, A.H. Ross, W.H. Clark, M. Herlyn, D. Herlyn, G. Maul, Z. Steplewski, H. Koprowski, Monoclonal antibody to a highly glycosylated protein reacts in fixed tissue with melanoma and other tumors, Hybridoma 4 (1985) 243–255. United States.
[15] M. Kondoh, M. Ueda, M. Ichihashi, Y. Mishima, Decreased expression of human melanoma-associated antigen ME491 along the progression of melanoma pre-canceroses to invasive and metastatic melanomas, Melanoma Res. 3 (1993) 241–245. England.
[16] K. Kudo, A. Yoneda, D. Sakiyama, K. Kojima, T. Miyaji, M. Yamazaki, S. Yaita, T. Hyodo, R. Satow, K. Fukami, Cell surface CD63 increased by up-regulated polylactosamine modification sensitizes human melanoma cells to the BRAF inhibitor PLX4032, Faseb. J. 33 (2019) 3851–3869.
[17] S. Yu, J. Chen, M. Quan, L. Li, Y. Li, Y. Gao, CD63 negatively regulates hepatocellular carcinoma development through suppression of inflammatory cytokine-induced STAT3 activation, J. Cell Mol. Med. 25 (2021) 1024–1034.
[18] B. Seubert, H. Cui, N. Simonavicius, K. Honert, S. Schäfer, U. Reuning, M. Heikenwalder, B. Mari, A. Krüger, Tetraspanin CD63 acts as a pro-metastatic factor via b-catenin stabilization, Int. J. Cancer 136 (2015) 2304–2315.
[19] B. Schoeps, C. Eckfeld, O. Prokopchuk, J. Böttcher, D. Häußler, K. Steiger, I.E. Demir, P. Knolle, O. Soehnlein, D.E. Jenne, C.D. Hermann, A. Krüger, TIMP1 triggers neutrophil extracellular trap formation in pancreatic cancer, Cancer Res. 81 (2021) 3568–3579.
[20] Q. Huang, Y.-J. Shen, C.-Y. Hsueh, Y. Guo, Y.-F. Zhang, J.-Y. Li, L. Zhou, miR-17-5p drives G2/M-phase accumulation by directly targeting CCNG2 and is related to recurrence of head and neck squamous cell carcinoma, BMC Cancer 21 (2021) 1074.
[21] X. Yin, S. Wanga, A.L. Fellows, J. Barallobre-Barreiro, R. Lu, H. Davaapil, R. Franken, M. Fava, F. Baig, P. Skroblin, Q. Xing, D.R. Koolbergen, M. Groenink, et al., Glycoproteomic analysis of the aortic extracellular matrix in marfan patients, Arterioscler. Thromb. Vasc. Biol. 39 (2019) 1859–1873. United States.
[22] Q. Huang, C. Hsueh, Y. Guo, X. Wu, J. Li, L. Zhou, Lack of miR-1246 in small extracellular vesicle blunts tumorigenesis of laryngeal carcinoma cells by regulating Cyclin G2, IUBMB Life 72 (2020) 1491–1503.
[23] Q. Huang, C.-Y. Hsueh, Y.-J. Shen, Y. Guo, J.-M. Huang, Y.-F. Zhang, J.-Y. Li, H.-L. Gong, L. Zhou, Small extracellular vesicle-packaged TGFβ1 promotes the reprogramming of normal fibroblasts into cancer-associated fibroblasts by regulating fibronectin in head and neck squamous cell carcinoma, Cancer Lett. 517 (2021) 1–13.
[24] F. Varghese, A.B. Bukhari, R. Malhotra, A. De, IHC profiler: an open source plugin for the quantitative evaluation and automated scoring of immunohistochemistry images of human tissue samples, in: S.A. Aziz (Ed.), PLoS One 9 (2014), e96801.
[25] M. Kang, J. Ryu, D. Lee, M.-S. Lee, H.-J. Kim, S.H. Nam, H.E. Song, J. Choi, G.-H. Lee, T.Y. Kim, H. Lee, S.J. Kim, S.-K. Ye, et al., Correlations between transmembrane 4 L6 family member 5 (TM4SF5), CD151, and CD63 in liver fibrotic phenotypes and hepatic migration and invasive capacities, in: R.B. Ray (Ed.), PLoS One 9 (2014), e102817.
[26] H. Koh, H. An, J. Jung, D. Song, The prognostic significance of CD63 expressionin patients with non-small cell lung cancer, pjp 70 (2019) 183–188.
[27] W. Liu, X. Li, X. Zhu, M. Hou, W. Zhao, CD63 inhibits the cell migration and invasion ability of tongue squamous cell carcinoma [Internet], Oncology Letters (2018) [cited 2020 Jun 10]; Available from: http://www.spandidos-publications.com/10.3892/ol.2018.8499.
[28] N. Tominaga, K. Hagiwara, N. Kosaka, K. Honma, H. Nakagama, T. Ochiya, RPN2-mediated glycosylation of tetraspanin CD63 regulates breast cancer cell malignancy, Mol. Cancer 13 (2014) 134.
[29] M. Kase, A. Adamson, M. Saretok, A. Minajeva, M. Vardja, T. Jõgi, T. Asser, J. Jaal, Impact of tumor infiltrating CD63 positive cells on survival in patients with glioblastoma multiforme, J. Neurosurg. Sci. 60 (2016) 417–423. Italy.
[30] R. Vinod, R. Mahran, E. Routila, J. Leivo, K. Pettersson, K. Gidwani, Nanoparticle-aided detection of colorectal cancer-associated glycoconjugates of extracellular vesicles in human serum, Int. J. Mol. Sci. (2021) 22.
[31] Z. Song, J. Mao, R.A. Barrero, P. Wang, F. Zhang, T. Wang, Development of a CD63 aptamer for efficient cancer immunochemistry and immunoaffinity-based exosome isolation, Molecules 25 (2020).

[32] T. Yoshida, H. Ebina, Y. Koyanagi, N-linked glycan-dependent interaction of CD63 with CXCR4 at the Golgi apparatus induces downregulation of CXCR4, Microb. Immunol. 53 (2009) 629–635. Australia.
[33] M. Ageberg, A. Lindmark, Characterisation of the biosynthesis and processing of the neutrophil granule membrane protein CD63 in myeloid cells, Clin. Lab Haematol. 25 (2003) 297–306. England.
[34] K.-K. Jung, X.-W. Liu, R. Chirco, R. Fridman, H.-R.C. Kim, Identification of CD63 as a tissue inhibitor of metalloproteinase-1 interacting cell surface protein, EMBO J. 25 (2006) 3934–3942.
[35] H. Suárez, Z. Andreu, C. Mazzeo, V. Toribio, A.E. Pérez-Rivera, S. López-Martín, S. García-Silva, B. Hurtado, E. Morato, L. Peláez, E.A. Arribas, T. Tolentino-Cortez, G. Barreda-Gómez, et al., CD9 inhibition reveals a functional connection of extracellular vesicle secretion with mitophagy in melanoma cells [Internet], J. Extracell. Ves. (2021) [cited 2021 Jun 9]; 10. Available from: https://onlinelibrary.wiley.com/doi/10.1002/jev2.12082.
[36] P. Sharma, S. Alsharif, A. Fallatah, B.M. Chung, Intermediate filaments as effectors of cancer development and metastasis: a focus on keratins, Vimentin, and nestin, Cells 8 (2019).
[37] V. Karantza, Keratins in health and cancer: more than mere epithelial cell markers, Oncogene 30 (2011) 127–138.
[38] S.A. Joosse, J. Hannemann, J. Spötter, A. Bauche, A. Andreas, V. Müller, K. Pantel, Changes in keratin expression during metastatic progression of breast cancer: impact on the detection of circulating tumor cells, Clin. Canc.Res. 18 (2012) 993–1003. United States.
[39] W. Han, C. Hu, Z.-J. Fan, G.-L. Shen, Transcript levels of keratin 1/5/6/14/15/16/17 as potential prognostic indicators in melanoma patients, Sci. Rep. 11 (2021) 1023.